Limnol. Oceanogr., 48(1, part 2), 2003, 557–567

Remote assessment of benthic substrate composition in shallow waters using multispectral reflectance

P. Jeremy Werdell[1] *and Collin S. Roesler*[2]
Department of Marine Sciences, University of Connecticut, 1084 Shennecossett Road, Groton, Connecticut 06340

Abstract

We investigated the utility of quantifying percent coverage of benthic substrate constituents from surface multispectral reflectance measurements. Six substrates were considered: kelp, eelgrass, clay, silt, mineralic sand from a temperate environment, and turtlegrass and carbonate sand from a tropical environment. Each had a unique albedo spectrum that contributes differently to the upward light field in an optically shallow environment. Simplifications to the radiative transfer equation yield an analytic solution for surface reflectance in optically shallow environments. The objectives were to test the inverse model to predict bottom albedo from measurements of surface reflectance, diffuse attenuation, and water depth in the turbid water of eastern Long Island Sound, Connecticut, and clear waters off Exuma, Bahamas. A linear mixing model was used to deconvolve the derived albedo spectra into contributions by the six constituents. The inverse and deconvolution models accurately identified the dominant substrate in the six homogeneous habitats (single point determinations) and predicted the gradient in substrate composition along transects. This approach has applications to benthic survey mapping, habitat assessment, and habitat monitoring.

Coastal, estuarine, and inland waters support a diverse assortment of benthic communities and ecosystems, many of which possess both commercial and ecological value. Climatic disturbances, erosion, industrial pollution, and dredging may alter the physical characteristics and composition of benthic ecosystems, frequently resulting in species diversity changes. These have broader impacts on local fisheries, industrial and private development, and water quality. Periodic assessment of the abundance and health of the submerged marine and intertidal communities is needed to improve our scientific understanding of perturbation responses by benthic ecosystems and our ability to manage delicate marine resources (Snedaker and Getter 1985; Dennison et al. 1993; Clark 1996).

A number of techniques exist for monitoring the benthos of shallow waters. SCUBA-based surveys provide great accuracy and high resolution (Luckhurst and Luckhurst 1978; Schneider et al. 1987) yet are limited by the time and manpower necessary to monitor large bodies of water and long stretches of coastline. Acoustic techniques, such as the ultrasonic signal processor (Roxanne), have been successful in determining the geological composition of the sea floor (e.g., silts and clays, sand, gravel, and rock; Chivers et al. 1990; Schlagintweit 1993). However, they are not effective at identifying the composition or even the presence of submerged aquatic vegetation such as seagrasses and seaweeds. Color aerial photography has been used to monitor and map benthic environments in shallow waters, particularly seagrass meadows (Benton and Newman 1976; Austin and Adams 1978; Orth and Moore 1983; Kirkman et al. 1988; Ferguson et al. 1993; Sheppard et al. 1995). However, much of the interpretation of aerial photographs is based upon brightness. Shallow submerged aquatic vegetation appears dark and is often indistinguishable from deep water. Variable water clarity, bottom sediments, macroalgae, epiphytes, and shell hash add to the uncertainty in photographic identification of seagrass habitats.

Remotely operated and autonomous underwater vehicles, towed camera sleds, and crewed submersibles have proved to be useful for obtaining macrofaunal population estimates and identifying microhabitat features, such as biogenic depressions, sand wave crests, and boulders, with high resolution and in virtually all environments (e.g., Felley et al. 1989; Langton and Uzmann 1989; Malatesta et al. 1992). The trade offs are the time and manpower required to conduct such surveys and vagaries in automated image analysis.

Remotely sensed ocean color data have been implemented to identify and map submerged aquatic vegetation in optically shallow waters (Lyzenga 1978; Savastano et al. 1984; Ackleson and Klemas 1987; Spitzer and Dirks 1987; Armstrong 1993; Luczkovich et al. 1993; Zainal et al. 1993; Mumby et al. 1997). This is possible because a fraction of the radiant flux that enters the ocean propagates to the bottom, is modified by the absorption and scattering properties of the substrate, and propagates back to the surface containing spectral information about the substrate. As such, a number of models have been developed that describe irradiance reflectance as a function of bottom albedo and water depth (Gordon and Brown 1974; Ackleson and Klemas 1986; Philpot 1987; Mobley et al. 1993; Lee et al. 1994; Maritorena et al. 1994; Leathers and McCormick 1998; Lee et al. 1998, 1999).

[1] Current address: Science Systems and Applications, Incorporated, Goddard Space Flight Center, Code 970.2, Greenbelt, Maryland 20771.

[2] To whom correspondence should be addressed. Current address: Bigelow Laboratory for Ocean Sciences, 180 McKown Point, West Boothbay Harbor, Maine 04575.

Acknowledgments

Robert Whitlatch and Ralph Lewis provided helpful comments on an earlier version of the manuscript. The University of Connecticut Marine Science and Technology Center provided boat time for the Long Island Sound work. We thank two anonymous reviewers for constructive criticism. This project was supported by the Office of Naval Research, Environmental Optics Program, Maine Space Grant, and a graduate research assistantship (to P.J.W.) from the University of Connecticut.

Table 1. Notation.

A	Substrate albedo, dimensionless
b_{bd}	Backscattering coefficient for downward irradiance, m^{-1}
E_d, E_u	Downward and upward irradiance, subscripts *w* and *b* indicate contributions by water column and bottom, respectively, W m^{-2}
f	Substrate fractional coverage, dimensionless
H	Water depth, m
K_d, K_u	Diffuse attenuation coefficient for downward and upward irradiance, m^{-1}
R_D, R_H	Irradiance reflectance for an optically deep water column and an optically shallow water column of depth H, dimensionless
z	Depth measured downward from the surface, m
λ	Wavelength (subscript *c* indicates channel central wavelength), nm
τ	Optical depth for diffuse attenuation, dimensionless
$\wedge$	Estimated quantity, used as overstrike

Measured albedo is some combination of the substrate constituents' albedo spectra. The nature of the combination depends upon the spatial scales of constituents relative to the spatial scales for interactive scattering and absorption between constituents. When the spatial scales of constituent patchiness are large relative to these optical scales, the upward photons can be attributed primarily to scattering by a single constituent rather than multiple scattering between constituents. The resulting albedo can be expressed as a linear combination of the individual constituent albedo signatures, proportional to their percent aerial coverage (Adams et al. 1986, 1992; Johnson et al. 1991).

Here we develop a three-step modeling approach for estimating substrate composition. Our approach is to (1) use an analytical shallow-water reflectance model to extract a bottom albedo spectrum from surface reflectance, (2) deconvolve the bottom albedo spectrum into percent contributions by substrate components, and (3) compare the derived substrate composition with that determined by direct observation. We have chosen to test our approach in two optically distinct regimes with a range of benthic substrates: eelgrass (*Zostera marina*), kelp (*Laminaria agardhii*), mineralic sand and clay in turbid temperate waters of Long Island Sound (LIS), and carbonate sand and turtlegrass (*Thalassia sp.*) in clear tropical waters off Exuma, Bahamas (EB).

Approach

Model development—The subsurface upward light field in an optically shallow environment can be expressed as contributions arising from the water column and the bottom interface. Approximations to the radiative transfer equation yield a simple expression for each of these contributions (Lyzenga 1978; Philpot 1987; Maritorena et al. 1994). Briefly, the contribution by the water column is the vertically integrated contributions by each infinitesimal layer, δz, from the surface to the bottom at depth H (*see Table 1* for notation). Within layer δz at depth Z, a fraction of the downward irradiance, $E_d(Z)$, is redirected into the upward direction due to backscattering:

$$E_{uw}(Z) = b_{bd}(Z)E_d(Z)$$

where $b_{bd}(Z)$ is the backscattering coefficient for downward irradiance at depth Z. The downward irradiance at Z is the attenuated solar irradiance incident on the ocean, $E_d(0)$, where the zero in parentheses indicates depth at the surface just beneath the air/sea interface:

$$E_d(Z) = E_d(0)\exp\left[-\int_0^Z K_d(z)\,dz\right]$$

where $K_d(z)$ is the depth-dependent diffuse attenuation coefficient for downward irradiance. The upward irradiance originating at Z is attenuated as it propagates to the surface so that the contribution to upward irradiance at the surface by the layer at Z is

$$E_{uw}(Z \to 0) = E_{uw}(Z)\exp\left[-\int_Z^0 K_u(z)\,dz\right]$$

where $K_u(z)$ is the depth-dependent diffuse attenuation coefficient for upward irradiance. Integrating over all Z, from the surface to depth H, yields the total upward irradiance originating from the water column:

$$E_{uw}(0) = E_d(0)\int_0^H b_{bd}(Z)\exp\left[-\int_0^Z (K_d(z) + K_u(z))\,dz\right]dZ \quad (1)$$

The upward irradiance originating from the bottom interface is the reflected portion of downward irradiance incident on the benthic surface at depth H

$$E_{ub}(H) = AE_d(0)\exp\left[-\int_0^H K_d(z)\,dz\right]$$

where A is the albedo of the interface. This irradiance is attenuated as it propagates up to the surface, so

$$E_{ub}(0) = AE_d(0)\exp\left[-\int_0^H (K_d(z) + K_u(z))\,dz\right] \quad (2)$$

Adding Eqs. 1 and 2 yields the total upward irradiance. Approximations that the diffuse attenuation coefficients and b_{bd} are not depth dependent, and that $K_u = K_d$, yield a simple analytic solution for the upward light field at the surface:

$$E_u(0) = E_d(0)\left[\frac{b_{bd}}{2K_d}(1 - \exp(-2K_dH)) + A\exp(-2K_dH)\right] \quad (3)$$

For an infinitely deep ocean (i.e., where $H \to \infty$) the ratio of the upward to downward irradiance is defined to be the irradiance reflectance for optically deep water, R_D. This boundary condition applied to Eq. 3 demonstrates that the ratio of b_{bd} to $2K_d$ equals R_D. Thus, the subsurface irradiance

reflectance, the ratio of $E_u(0)$ to $E_d(0)$ measured just beneath the surface over an optically shallow-water column of depth H, is

$$R_H = R_D + (A - R_D)\exp(-2K_dH) \quad (4)$$

Inversion of Eq. 4 yields an analytic expression for the bottom albedo as a function of measured subsurface reflectance spectra:

$$A = R_D + (R_H - R_D)\exp(2K_dH) \quad (5)$$

Several simplifying assumptions were incorporated into the derivation of the forward model in order to ensure that the analytical solution was expressed as a function of measurable quantities. These assumptions include K_u and K_d are depth independent, $K_u = K_d$, and K_u does not vary in the presence of an optically shallow bottom. This requires that the water column is homogeneous with regard to the inherent optical properties (i.e., absorption and scattering) and that the angular distribution of the light field is invariant with depth. This may be true in the asymptotic region of the water column, but certainly not in the presence of hydrographic structure where the inherent optical properties are likely to vary and not in the presence of interfaces where the angular distribution of light will vary. Monte Carlo simulations and some empirical data were used to evaluate the assumptions in clear waters (Maritorena et al. 1994). We examine the variability in the diffuse attenuation coefficients and the effects on A retrieval in the turbid waters.

Constraints of spectral optical depth—All of the terms in Eq. 5, save H, are spectrally dependent. The depth to which light penetrates also varies as a function of wavelength. Therefore, some spectral bands of R_H will be dominated by water column processes and contain little to no signature from the bottom substrate. The spectral optical depth for diffuse attenuation is

$$\tau = K_dH$$

From the sensitivity of the instrumentation used here (determined from dark current readings), the physical depths that exceeded $\tau > 3.5$ for any particular wavelength yielded a signal to noise ratio less than 3, which, when incorporated into the model, yielded unrealistic values for albedo due to the amplifying effect of attenuation. In all the LIS cases presented here, channels 412 and 443 nm were excluded from further analysis.

Deconvolution of spectral bottom albedo—Once A is derived via Eq. 5, it is mathematically deconvolved into contributions by unique substrates using a linear spectral mixing model (Sabol et al. 1990; Johnson et al. 1991):

$$A = \sum f_iA_i \quad (6)$$

where f_i is the fraction of coverage by substrate i and A_i is the laboratory measured A for substrate i. Coefficients f_i were determined by linear least squares regression constrained such that $f_i > 0$.

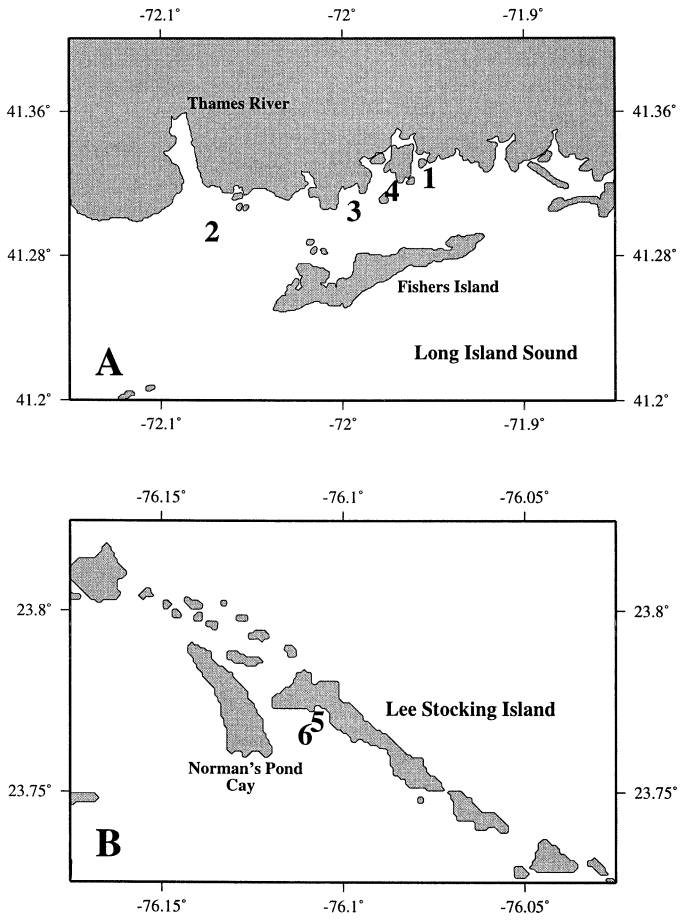

Fig. 1. Six sampling sites were located in (A) eastern Long Island Sound, Connecticut (LIS), and (B) waters near Lee Stocking Island, Exuma, Bahamas (EB). Benthic substrate composition consisted of: (1) a dense eelgrass (*Zostera marina*) meadow (H = 4.1 m), (2) a kelp (*Laminaria sp.*) forest (H = 3.0 m), (3) a mineralic sand bed (H = 3.8 m), (4) a mineralic clay/silt bed (H = 1.9 m), (5) a calcareous sand bed (H = 3.1 m), and (6) a mixed calcareous sand and turtlegrass (*Thalassia sp.*) meadow (H = 3.8 m).

Methods

Spectral reflectance—Shallow-water environments in eastern Long Island Sound and near Lee Stocking Island, Exuma, Bahamas, were selected to provide a range in benthic substrate compositions and water clarity (Fig. 1). Initial model testing was performed over spatially homogeneous sites dominated by a single substrate. At these six sites, profiles of downward and upward irradiance and upward radiance were made over each site with a seven-channel modular ocean color profiling and surface reference system (OCP200, Satlantic; λ_c = 410, 443, 490, 510, 555, 665, and 683 nm). Final model testing was performed along transects (~20 to 30 m) in each environment over a spatially inhomogeneous benthic substrate and variable water depth. For these measurements a profile of measurements was made at one point, as described above, and a seven-channel tethered spectral radiometer buoy (TSRB, Satlantic) was towed at a constant velocity along the transect. Two different TSRB instruments

were used with slightly different channel configurations (λ_c = 410, 443, 490, 555, 665, 683, and 705 nm in LIS and λ_c = 405, 410, 443, 490, 510, 555, and 665 nm in EB). A Datasondes altimeter simultaneously measured bottom depth. For all shallow sites and transects, bathymetric maps and charts of local currents were used to discern the flow of surface water masses between adjacent deep and shallow-water sites, minimizing the difference in water column properties between the paired sites. These optically deep sites were within 50 to 250 m of the optically shallow sites. Sites and transects were surveyed and photographed for comparison with model results. Samples of each substrate type were collected for laboratory analyses.

All measurements of irradiance and radiance were corrected for variations in solar irradiance using the surface deck sensor. Diffuse attenuation coefficients were calculated from profiles of radiance and irradiance using a nonlinear exponential fit to the corrected data. These coefficients were used to propagate all irradiance and radiance measurements to just beneath the surface; this correction is quite important for TSRB data, particularly in turbid waters. Upwelling radiance and irradiance were not corrected for instrument self-shading (Gordon and Ding 1992; Zibordi and Ferrari 1995); based upon the sun angle and absorption to scattering ratios the correction would be less than 3% (Leathers et al. 2001). Q factors, calculated from the ratio of the upward irradiance to the upward radiance, were used to convert the upward radiance, measured with the TSRB, to upward irradiance. These values ranged from 4.26 to 5.32 at 412 nm to 3.69 to 4.47 at 670 nm, decreasing monotonically with wavelength, with higher values observed over plant-dominated substrates and lower values over sand-dominated substrates. Surface reflectance spectra were calculated from the ratio of upward irradiance to downward irradiance.

Substrate sample analyses—Sample albedo was measured with a Cary 3E UV-visible spectrophotometer at 2-nm resolution over the wavelength range 300 to 850 nm using an integrating sphere in reflectance configuration. Measurements were calibrated to a known reflectance source during baseline correction.

The chlorophyll *a* (Chl *a*) concentration of eelgrass and sediment samples was measured spectrophotometrically after 48 h extraction in 90% acetone (Parsons et al. 1984). Concentrations are expressed per sample dry weight. Sediment samples were combusted at 550°C for 24 h. Initial and final weights were used to calculate dry weight or organic weight.

Results

Derivation of spectral albedo—Diffuse attenuation coefficients for upward and downward irradiance and upward radiance ranged from 0.2 to 0.9 m^{-1} and 0.05 to 0.5 m^{-1} over the spectrum, for LIS and EB, respectively (Fig. 2). Ninety-five percent confidence limits indicate that the attenuation coefficients did not vary significantly with depth, which was confirmed with piecewise calculations (data not shown). However, there was approximately 20% variation between the diffuse attenuation coefficients for upward and downward irradiance.

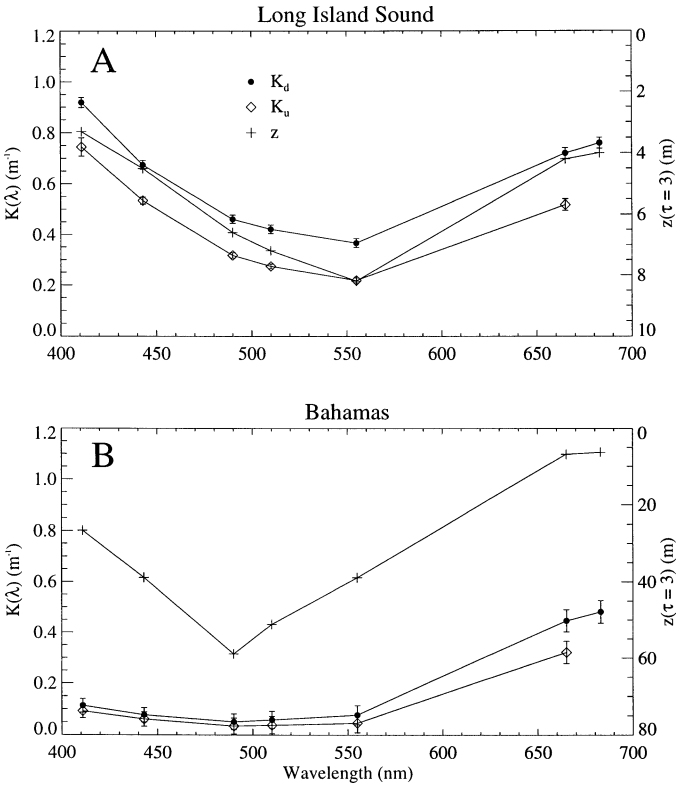

Fig. 2. Typical spectral diffuse attenuation coefficients for downward and upward irradiance in (A) Long Island Sound and (B) Exuma, Bahamas. Error bars indicated the 95% confidence limits on the nonlinear estimates. Physical depth for which $\tau = 3$ indicated by plus symbols, scale on right axis.

The penetration of light was very different for the two environments (Fig. 2). The limitation for resolving a bottom signature is that the water depth not exceed the depth at which $\tau < 3.5$. In LIS this constraint was approximately 3 to 8 m over the visible wavelength range, with maximal penetration to 8 m in the 555-nm band. Since the water depth for the sample sites varied from 2 to 6 m, only the channels in the 490- to 555-nm interval were within the optical depth constraint. EB waters were extremely clear by comparison. The sample sites varied in depth from 3 to 7 m, which for all the channels in the 410–555-nm waveband was well within the $\tau < 3.5$ constraint.

Surface reflectance spectra measured in optically shallow water, R_H, over the six homogeneous benthic substrates varied significantly in shape and magnitude (Fig. 3A,B). All reflectance spectra measured in LIS exhibited a maximum at 555 nm and had statistically different spectral shapes in the shorter wavelengths ($p < 0.05$, Student's *t*-test). The R_H spectra for EB waters were significantly different in shape, magnitude, and wavelength of maximal reflectance.

Surface reflectance spectra measured at the adjacent deep water sites, R_D, exhibited less variability in the red region of the spectrum (Fig. 3C,D). The R_D measured in LIS exhibited maximal values at 555 nm like those over optically shallow sites. The R_D measured in EB exhibited maximal reflectance values at 410 nm, significantly bluer than the R_H spectra.

Estimates of benthic albedo spectra, $\hat{A}$, were derived from

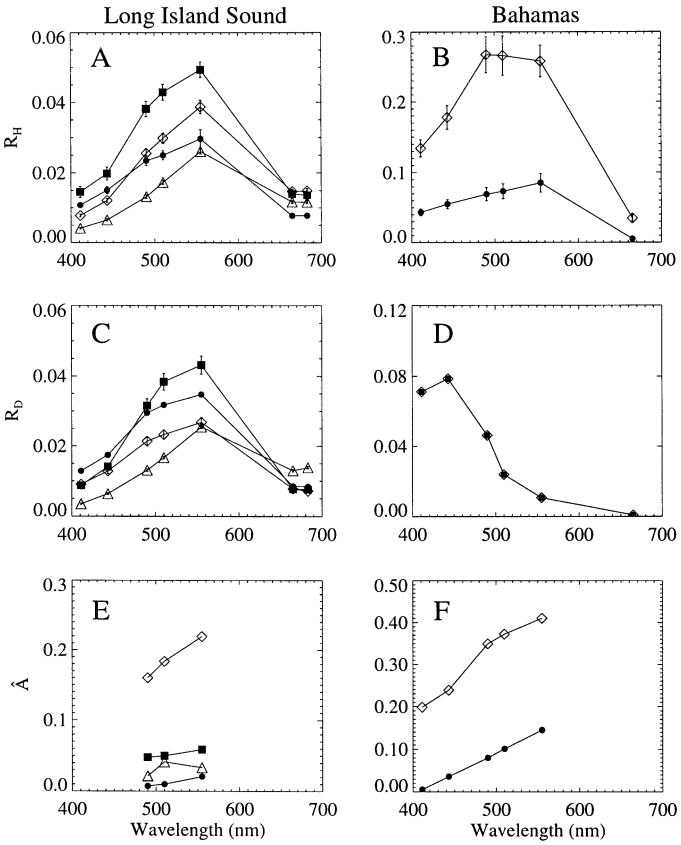

Fig. 3. Surface reflectance and albedo spectra for the six sampling stations in Long Island Sound and Exuma, Bahamas. (A) and (B) Spectral irradiance reflectance was measured just beneath the air/sea interface over the homogeneous substrates, (C) and (D) in adjacent optically deep water, and (E) and (F) the modeled spectral albedo from Eq. 5. Symbols indicate substrate type: temperate eelgrass (solid circles), kelp (solid squares), mineralic clay/silt (open triangles), and mineralic sand (open diamonds) in Long Island Sound and tropical turtlegrass (solid circles) and calcareous sand (open diamonds) in Exuma, Bahamas. Error bars in (A)–(D) indicate uncertainties in measurements. The two spectra in (D) were indistinguishable within the size of the symbols.

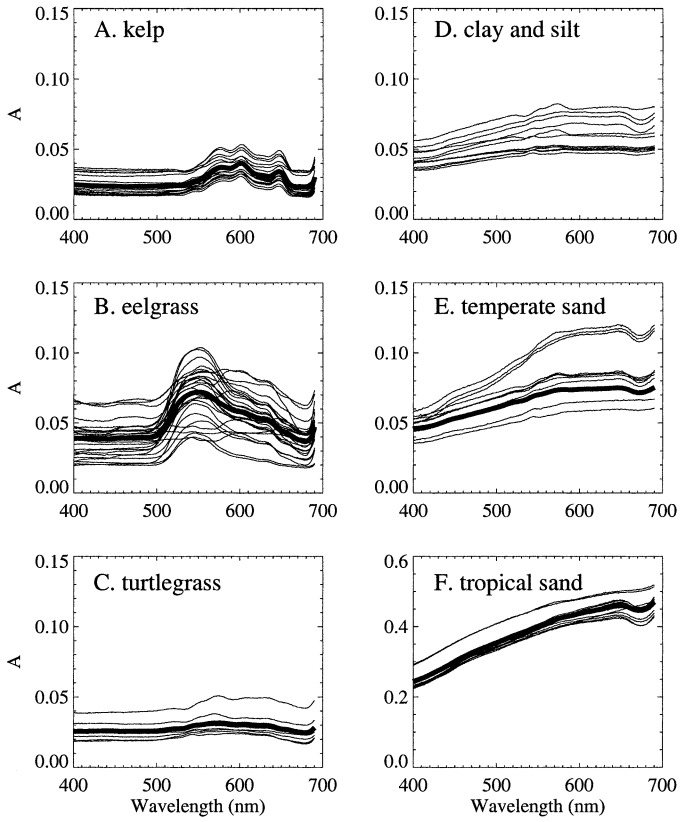

Fig. 4. Albedo spectra measured spectrophotometrically on discrete samples: kelp (n = 18), temperate eelgrass (n = 28), tropical turtlegrass (n = 7), mineralic clay/silt (n = 10), mineralic sand (n = 10), and tropical carbonate sand (n = 11; note scale change). Bold spectra are ensemble averaged albedo spectra used as end members in the linear least squares mixing model (Eq. 6).

Eq. 5 using the measurements of K_d, R_H, and R_D for wavebands within $\tau < 3.5$ (Fig. 3E,F). The spectra from LIS ranged from approximately 2% to 25% while those from EB ranged from 2% to 40%.

Spectral albedo for different substrates—Albedo spectra were measured for 7 to 28 samples of each substrate (Fig. 4) collected from the two environments. Plant albedo spectra exhibited the most spectral variations due to differences in pigment composition and concentration (Fig. 4, left panels). The spectral shape of the kelp albedo did not vary significantly between samples, although the brightness varied by a factor of two (Fig. 4A). Absorption by Chl *a* and *c* and fucoxanthin results in a reflectance window in the 560- to 660-nm range. Kelp fronds are very thick (~2 mm) and thus the spectral bands in which pigments absorb are virtually nonreflective. The variation in brightness appeared to be related to the quantity of a white epiphytic bryozoan. Eel grass contains the accessory pigment Chl *b* and lacks strong carotenoid absorption in the 500- to 600-nm range, which results in a broad reflectance window (Fig. 4B). The blades of eelgrass are thinner than the kelp fronds and thus there are more spectral variations due to variability in pigment packaging. Epiphytic growth on these blades also caused variations in the spectrally independent brightness of the albedo. Although turtlegrass and eelgrass have complementary pigment compositions, the turtlegrass blades appeared much darker to the eye than the temperate eelgrass, an observation consistent with the albedo measurements (Fig. 4C).

Sand albedo spectra are relatively featureless compared to the plant spectra (Fig. 4, right panels). The minor spectral features, in particular the absorption feature at 676 nm, indicates the presence of some Chl *a* and other accessory pigments associated with plant detrital material, benthic diatoms, and other microscopic plants. The average brightness and red to blue ratio ($A_{700}:A_{400}$) of the albedo increased from the temperate clay/silt (5% and 1.2) to the temperate sand (8% and 1.8) to the tropical sand (40% and 2.2; Fig. 4D–F). The mineralic sands, clays, and silt from LIS are composed primarily of quartz, feldspar, and mica (Lewis and Stone 1991) while the tropical sand is composed primarily of calcium carbonate. The tropical sand albedo is brighter but not whiter, despite the appearance to the eye. The sample

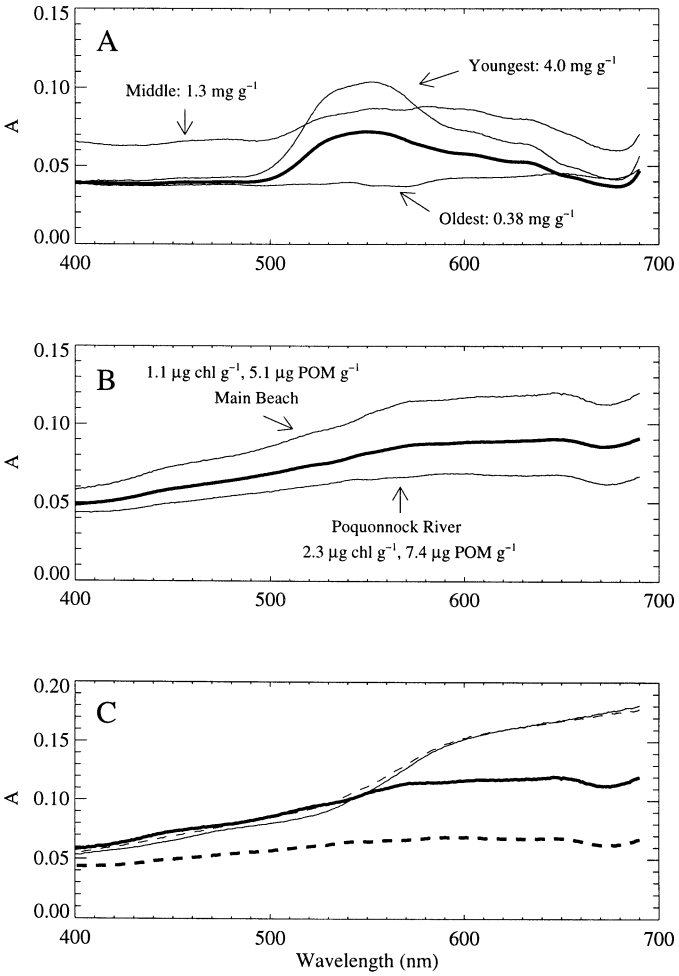

Fig. 5. Range of variability in substrate albedo spectra. (A) Age of eelgrass blades from the youngest inner to the oldest outer blades with associated dry-weight-specific Chl *a* concentrations and ensemble mean albedo spectra (bold, $n = 28$). (B) Organic content of temperate beach sand and river mouth clay/silt with dry-weight-specific Chl *a* and particulate organic matter concentrations, and mean albedo spectra (bold, $n = 20$). (C) Effects of combustion on the albedo of mineralic sediment. Beach and river bottom sand from (B) before (bold solid and dashed, respectively) and after (thin solid and dashed, respectively) combustion.

averaged albedo spectra (bold lines) were used in the linear least squares albedo mixture model, Eq. 6.

Eel grass exhibited the largest spectral variability in albedo of the plant substrates (Fig. 5A). The largest albedo was measured on the youngest, innermost plant blades with the highest dry-weight-specific Chl *a* concentration. As the blade ages, the pigment concentration decreases, flattening the albedo spectral shape. Epiphytes and attached algae concentrations increase as blades age (Neckles et al. 1993; Williams and Ruckelshaus 1993; Heck et al. 2000) causing the observed spectrally independent brightening of the middle blades. Once the oldest outer blades begin to die, the Chl *a* concentration decreases, and the albedo darkens.

Albedo of mineralic sediments from LIS varied by a factor of 3, from spectrally flat (clay/silt collected from the mouth of the Poquonock River inshore of site 3) to linearly increasing toward the red end of the spectrum (sand collected from Main Beach, inshore and west of site 3). Eighty four percent of the grains in the mineralic sand samples were greater than 250 μm, while 70% of the grains in the mineralic clay/silt sample were less than 70 μm (where grain size defines sand versus clay and silt, Lewis 1984). As these temperate sand and clay/silt sediments are of the same composition (Lewis and Stone 1991), the flattening darkening of the albedo spectra is likely due to absorption by bacterial and other organic coating. The larger surface area to volume ratio of the smaller grains would provide greater substrate surface for such coatings, as was observed (Fig. 5B). Once the organic material was removed by combustion, there was no observable difference between the coarse- and fine-grained sediment albedo spectra, confirming their common composition. Both a significant increase in the albedo spectra in the 550- to 750-nm range for both samples and an increase in the blue band albedo for the fine-grained sample were observed (Fig. 5C), bringing the albedo of both samples to magnitudes and spectral shapes like those of the brightest temperate sand samples (Fig. 4). Thus the albedo of sediments was observed to be a continuum between organic coated clays, with the lowest and flattest albedo, to relatively clean mineralic sands, with brighter and redder albedo spectra.

Substrate identification at homogeneous sites—The linear albedo mixture model was applied to each derived albedo spectrum (Table 2). The largest model-estimated fraction was always associated with the observed dominant substrate. The contributions by substrates other than the dominant one

Table 2. The estimate of the areal coverage fraction derived from linear least squares regression analysis, Eq. 6, and coefficient of determination, r^2, for the regression; na indicates substrate not used in analysis. Observed percentages shown in parentheses; ds indicates only the dominant substrate was determined visually, secondary contributors were not quantified.

Observed dominant substrate	$f_{\text{eel grass}}$	f_{kelp}	$f_{\text{mineralic sand}}$	$f_{\text{turtle grass}}$	$f_{\text{carbonate sand}}$	r^2
Eel grass	1.00 (1)	0.00 (0)	0.00 (0)	na	na	0.81
Kelp	0.02	0.69 (ds)	0.29	na	na	1.00
Mineralic sand	0.27	0.00 (0)	0.73 (ds)	na	na	0.98
Mineralic clay/silt	0.07	0.00 (0)	0.93 (ds)	na	na	0.16
Turtle grass	na	na	na	0.57 (0.55)	0.43 (0.45)	0.81
Carbonate sand	na	na	na	0.00 (0)	1.00 (1)	0.95

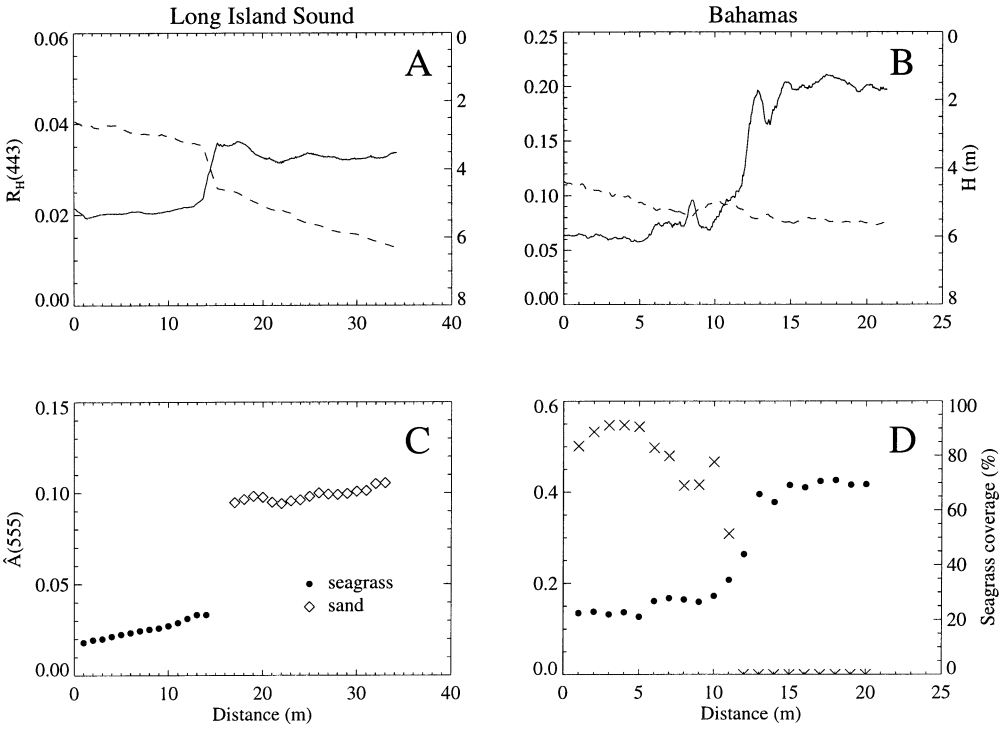

Fig. 6. Radiometric and bathymetric measurements and modeled albedo along Long Island Sound and Exuma, Bahamas, transects. (A) and (B) Surface irradiance reflectance at 443 nm (solid line) and water depth (dashed line) as a function of distance along the transect. (C) Modeled albedo at 555 nm over eelgrass and sand substrates. (D) Modeled bottom albedo at 555 nm (filled circles) and calculated percent coverage of turtlegrass (cross symbols).

were on the order of <30% in all cases for LIS sites and for the EB sand site. The estimates for the EB turtlegrass site were a 57% to 43% ratio of turtlegrass to sand, which compared well to the observation that 45% of the sand was visible through the turtlegrass meadow (we could not find a turtlegrass meadow without significant sand coverage). The coefficient of determination, r^2, indicates that in all cases, except the clay/silt site, >80% of the observed variation in the $\hat{A}$ was explained by the linear mixture model. The low r^2 for the clay/silt site is due to the high value of $\hat{A}(510)$; this did not, however, prevent the model from predicting the correct dominant substrate.

Substrate identification along transects—Measured surface reflectance varied in brightness along the transect but was not generally covariant with bathymetry for either environment (Fig. 6A,B). While there was a step function in both the R_H at 443 nm and bottom depth along the LIS transect, the trend in depth was not associated with a trend in R_H. Similarly, a step function in R_H occurred along the EB transect with no similar trend in water depth. The derived albedo spectra along the transects provide much more information about the underlying substrate than does surface reflectance.

The TSRB used in LIS did not have sufficient channels in the green wavebands to resolve $\hat{A}$ at three wavelengths, the minimum necessary to distinguish kelp from eelgrass or sand from clay/silt. However, the changes in the magnitude of derived albedo were sufficient to distinguish between sediments and plant substrates (Fig. 6C). The derived albedo at 555 nm was constant and approximately 2–3% over the shallow portion of the transect; the increase in water depth at ~15 m along the transect was associated with a factor of 3 increase in albedo. This is consistent with a transition from a plant-dominated to a sediment-dominated substrate, which was confirmed by direct observation. We note that the plant density decreased along the transect, yielding more of the underlying sand and accounting for the slight brightening. At the end of the transect (32–33 m) we observed a pile of shell hash, which may account for the slight brightening.

The water clarity at the EB site resulted in $\hat{A}$ spectra with five channel resolution (415 to 555 nm), which was sufficient for the mixture model (Fig. 6D). $\hat{A}$ at 555 nm was low at the shallow end of the transect, increasing toward the deep end with a step-wise increase at ~10 m. The derived substrate composition indicated that as the water depth increased over the transect, the contribution of turtlegrass decreased from approximately 45% to <5%. The transition was confirmed visually; no turtlegrass was observed in the sand but half of the coverage in the turtlegrass meadow was sand.

Sensitivity analysis of albedo derivation—The sensitivity of $\hat{A}$ to variability in the input parameters was assessed for observed ranges in those parameters using a bootstrap approach. The water depth, as determined by the altimeter, was allowed to vary by ±10%, which accounts for the resolution of the instrument as well as the variability that arises from spatial averaging (Fig. 7A). This source of variability had

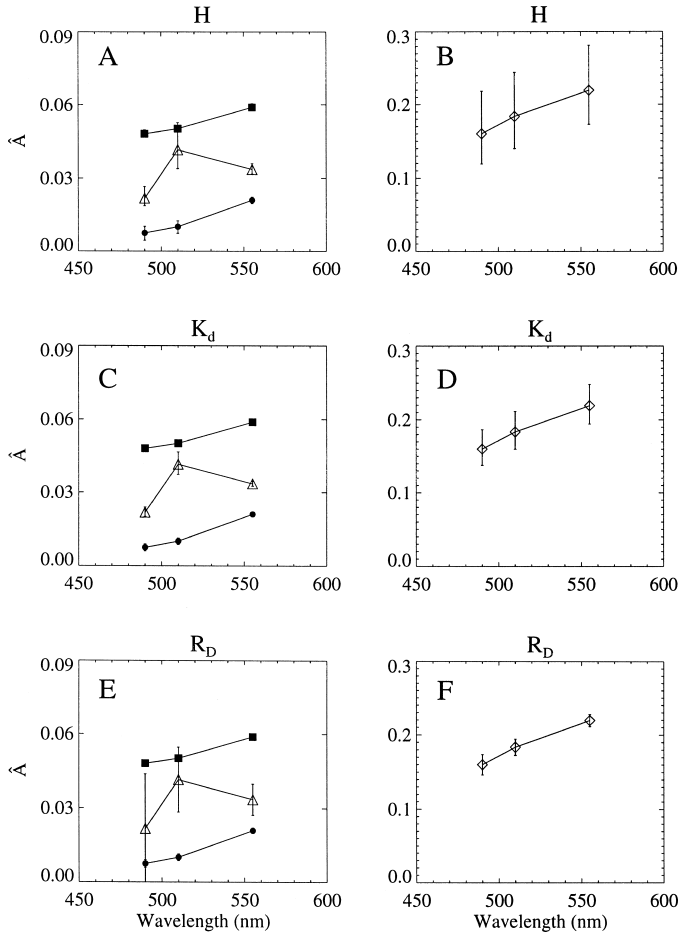

Fig. 7. Sensitivity analysis of the inverse model. Error bars indicate standard deviation of modeled albedo resulting from variation (values in parentheses) in input parameters at the Long Island Sound sites. (A) and (B) Water depth (10%), (C) and (D) K_d (5%), and (E) and (F) R_D (2%). Symbols as in Fig. 3; (A), (C), and (E) show kelp, eelgrass, and clay/mud; (B), (D), and (F) show temperate sand cases.

the largest impact on the derived $\hat{A}$ for the sand site (Fig. 7B). The uncertainty was approximately 25% in magnitude. The 95% confidence limits for K_d represented a 2 to 5% variation in the derived spectrum; this translated into a very small source of uncertainty in $\hat{A}$ for the eelgrass, kelp, and clay/silt sites (Fig. 7C) and a 15% uncertainty for the sand site (Fig. 7D). Measurement errors in R_D were observed to be $\pm 2\%$. These exhibited virtually no effect on $\hat{A}$ except at the clay/silt site at the 490- and 510-nm channels (Fig. 7E,F). The $\hat{A}$ spectra were statistically distinct from one another in spite of the uncertainty in the input parameters.

Discussion

The spectrum of light emanating from the ocean surface in shallow waters contains information on the optical properties of the seawater constituents and the benthic substrate. The challenges for extracting substrate composition from surface reflectance lie in the removal of the water column signal and in the interpretation of the substrate signal into constituent aerial coverage. The degree of difficulty in these challenges depends, in part, on the instrumental spectral resolution, but more importantly on the spectral uniqueness and relative strengths of the signals arising from the water and the substrate. In optically clear waters with a bright sand bottom, the benthic albedo can dominate the surface reflectance signal. This greatly simplifies the retrieval of the albedo using the inverse model of Maritorena et al. (1994). In the temperate turbid waters of LIS, where the bottom albedo is not as bright as that for carbonate sand and the diffuse attenuation in the water column is very large, the benthic albedo can contribute less than 10% to the measured surface reflectance signature. The problem is compounded by a green water column over a plant-dominated substrate. The changes in brightness and spectral shape associated with the water column are not different from those induced by variations in the benthic substrate. This presents challenges for the model inversion. However, removing the effects of the water column and water depth yields spectral signatures associated with the benthic substrate. Within these spectral signatures lie the potential for interpretation of complex substrate composition from albedo.

Photographic or quasitrue color imagery, which relies on interpretation of scene brightness and color alone, cannot be decomposed into complex composition. In optically clear waters like EB, a transition from bright blue to dark blue indicates sand substrate and a deepening water column; a transition from bright blue to dark green indicates a shift from sand to turtlegrass substrate; a transition from dark blue to dark green indicates a shift from deep sand to turtlegrass, likely a shallowing water column due to the ecological niche of the plants. In LIS, a transition from bright green to dark green has multiple interpretations as a function of substrate and water depth. The goal of reflectance inversion approaches to habitat assessment is to unambiguously interpret changes in brightness and color with respect to water depth and substrate composition. The ease of routine optical assessment of shallow habitats could lead to improved spatial and temporal coverage of coastal monitoring programs aimed at investigating habitat complexity, diversity, and change.

We observed a significant increase in brightness along the transects with a corresponding increase (LIS) or no change (EB) in water depth. At the homogeneous substrate sites, maximal R_H values varied by a factor of 2 to 3 within each environment. At the EB site the increased brightness was due to a brightening of the albedo due to sand coverage. The interpretation was not so straightforward in LIS since the R_H brightness was only weakly correlated with the derived $\hat{A}$ brightness (rank correlation $r = 0.6$, $n = 4$) and there was no difference in the wavelength of maximal reflectance (i.e., chromaticity or perceived color).

The success of albedo retrieval in turbid water depends, to a greater degree, on the accuracy and precision of the reflectance, attenuation, and depth measurements than it does in clear waters. While the inversion has been shown to be robust in simulations of clear waters (Maritorena et al. 1994), it has not been examined in turbid waters, nor has it been applied to any real data. Finally, underwater substrate composition has not previously been retrieved from derived

albedo. Our goals were (1) to examine the robustness of the inversion model applied to measurements from turbid waters compared to clear waters and (2) test a deconvolution model to retrieve substrate composition from the derived albedo. Despite the dominance of the water column optical properties to the surface reflectance in optically shallow turbid waters, inversion resulted in reasonable values for benthic albedo spectra. The retrieval was most sensitive to the accuracy in water depth, which influences the term $[(R_H - R_D)\exp(2K_dH)]$. In turbid environments a water depth of 5 to 8 m is considered optically shallow, while in clear environments a depth of 40 to 50 m can be considered optically shallow for some wavelengths. Resolving water depth measurements within 10 to 50 cm represents nearly 10% uncertainty in turbid waters compared to 1% uncertainty in clear waters, which translates into a 15% versus 2.5% coefficient of variation in the exponential term.

The accuracy of the R_D measurements directly affects the accuracy of the $\hat{A}$ retrieval because R_D and $\hat{A}$ are equivalent to first order (i.e., the first term in Eq. 5). The accuracy becomes very critical when R_H and R_D are very similar (which indicates either that the bottom has small albedo values or that it is optically deep), particularly if the bottom is approaching the limiting optical depth and the exponential term is large. Small uncertainties in R_D lead to large uncertainties in $\hat{A}$ as $\tau \rightarrow 3.5$, as was the case for the kelp bottom.

The 95% confidence limits on the derived values for K_d and K_u represented 2% to 5% of the measured values and varied spectrally. That degree of uncertainty did not give rise to large errors in $\hat{A}$. Thus for our cases, the assumption that K_d was invariant with depth was not critical. A 20% variation, which is the order of uncertainty of the assumption $K_d + K_u = 2K_d$, yields variations in derived A that are larger than those with 5% variations; however, the derived $\hat{A}$ spectra are still significantly different from one another except between the clay/silt and the kelp stations at 555 nm (data not shown). The importance of being able to assume that water column attenuation coefficients for the upwelling and downwelling light fields could be approximated by a depth invariant value of K_d lies in the potential for extending this approach into a purely remote sensing technique, with no requirements for profiling or in situ instrumentation. If the approximation holds, all parameters in the inversion can be determined from surface, ship deck, or aircraft-borne sensors.

It is not possible to measure directly A in situ without the effects of the overlying water column and without some instrument shading effects. That the inversion gave rise to reasonable $\hat{A}$ values can only be verified by comparison with the laboratory A measurements under conditions of a homogeneous and known substrate composition. The deconvolution model makes use of the observation that each substrate has a unique spectral signature and that the wavelength resolution of the instruments is sufficient to detect the unique signature. The limited number of wavelengths at which $\hat{A}$ was retrieved presented a difficult test for deconvolution and forced the selection of a single albedo for each substrate. However, even with three wavelengths the deconvolution of $\hat{A}$ resulted in the correct determination of the dominant substrate.

The six sites were chosen such that the albedo could be attributed to one constituent. Even under these guidelines it is very difficult to find this situation in a natural environment. Only the eelgrass and carbonate sand sites represented homogeneous single-component substrates. The eelgrass meadow was in ~4 m water, with the top of the plants at ~2 m. The plant density was such that the bottom was not visible and thus only the eelgrass would contribute to A. The carbonate sand site had no plants and was in a dynamic area where organic detrital material would not settle and accumulate. The deconvolution model yielded results confirming 100% coverage of these respective end members. In the other cases, the observations were not as straightforward. That the model results indicated mixed substrate composition with a single dominant component is actually a more realistic result than a result of 100% coverage in these cases, due to the complex ecology of benthic substrates. The model did confirm what we observed about these constituents. Kelp and eelgrass rarely cooccur and were not observed to cooccur in our study sites; the model confirmed this as well. Kelp plants anchor to rocky substrates, with a plant density much lower than that observed for the eelgrass meadow. Thus the retrieval of 30% sand component coverage is expected, although we would interpret this as a rocky substrate since kelp does not grow in sandy bottoms. Similarly, the maximum height of turtlegrass plants is ~10 cm, so that the underlying sand between the plants is clearly visible. The estimated aerial coverage from in situ photographs was 55% turtlegrass and 45% sand, confirmed by the albedo model. Finally, the estimated coverage in mineralic sand and clay/silt sites included a fraction of the plant end members. Both of these sediment sites would contain benthic algae and phytodetritus (the latter was observed in a particle-rich layer skimming the surface in the benthic boundary layer). Thus the model estimates are likely a better reconstruction of the substrate than were the visual observations. What is often recorded by eye are large regions of recognizable constituents; what is determined by image analysis (e.g., random-point-intercept technique; Malatesta et al. 1992; Wahle and Peckham 1999) is dependent upon the relative scales of the image and the patch sizes. The albedo approach does not contain these biases and, by examining residuals of the deconvolution model, might even predict constituents that were not included in the original regression, thereby improving our understanding of the ecology of these habitats.

These are very encouraging results because the LIS experimental site represented a challenging test compared to the EB site: the LIS substrates (i.e., kelp, eelgrass, and mineralic clay/silt and sand) all had relatively low A values compared to carbonate sand; the water depth for each site was in the range of $\tau > 2$; only three wavelengths were used; and those wavelengths were not optimized to discern the largest differences in the substrate albedo spectra. Alleviating one or all of these limitations (i.e., environments for which there is a brighter substrate albedo or decreased attenuation with respect to water depth, instrumentation with increased spectral resolution, or more channels in the 500- to 650-nm range) would substantially improve the accuracy of the derived substrate composition by increasing the benthic to water signal ratio, by increasing the signal to noise

ratio, or by including spectral regions in which the largest differences between substrate albedo are observed.

Field radiometers are not designed specifically for benthic recognition surveys. The multispectral instruments used in this study were designed to provide data for pigment retrieval and satellite ocean color data product validation. Despite the limitations, we found that the existing ocean color sensors can provide useful information for benthic surveys in both clear and turbid water. Additional channels or hyperspectral instrumentation would dramatically improve the approach by providing additional degrees of freedom (thus more end members in the mixing model) and better resolution of the unique features in substrate albedo. That kelp, eelgrass, and sand can be distinguished from changes in the spectral slope from 500 to 550 nm is impressive. However, if channels in the 550- to 650-nm range were added, the potential for discerning peaks associated with chlorophytic versus chromophytic pigments would be possible (as seen in the measured hyperspectral albedo). This would lead to enhanced accuracy of substrate determination as well as the capability of resolving albedo variations within each substrate, such as those found in the eelgrass and sediment samples. We have demonstrated that albedo is very sensitive to such biogeochemical properties as leaf chlorophyll content and sediment organic and chlorophyll concentrations, with very predictable changes in the spectral shape. While we could only resolve substrate type with three wavelengths, more spectrally resolved measurements combined with a deconvolution model with more end members would provide the means to distinguish healthy productive marine plants from stressed or unhealthy plants, clean or scoured mineralic sand from organic-laden sediment, sediments rich in benthic algae from those without.

Our goal was to develop a viable technique using remotely sensed ocean color data for bottom recognition surveys in shallow waters. Such methods provide a spatial and temporal resolution that far exceeds most conventional, more invasive approaches such as diver surveys and submerged instrumentation. Coastal aquatic ecosystems possess both commercial and ecological value, and therefore periodic assessment of their health and abundance is beneficial to the local and global community. The methods presented here offer a useful approach for shallow-water regulatory activities by providing an inexpensive method of monitoring on large spatial and temporal scales with versatile deployment options for buoy, ship, and aircraft-based platforms. That we found accurate results in both very turbid and very clear waters, with minimal wavelength resolution, confirms that this approach will be applicable to a range of environments with varying water column and benthic optical properties. Further, accuracy will increase as the spectral resolution increases to incorporate the spectral bands of largest constituent albedo variability, thereby improving the capability for distinguishing those constituents.

References

ACKLESON, S. G., AND V. KLEMAS. 1986. Two-flow simulation of the natural light field within a canopy of submerged aquatic vegetation. Appl. Opt. **25:** 1129–1136.

———, AND ———. 1987. Remote sensing of submerged aquatic vegetation in lower Chesapeake Bay: A comparison of Landsat MSS to TM imagery. Remote Sens. Environ. **22:** 235–248.

ADAMS, J. B., M. O. SMITH, AND A. R. GILLESPIE. 1992. Imaging spectroscopy: Interpretation based on spectral mixture analysis, p. 145–166. *In* C. M. Pieters and P. Englert [eds.], Remote geochemical analysis: Elemental and mineralogical composition. Cambridge Univ. Press.

———, ———, AND P. E. JOHNSON. 1986. Spectral mixture modeling: A new analysis of rock and soil types at the Viking Lander 1 site. J. Geophys. Res. **91:** 8908–8112.

ARMSTRONG, R. A. 1993. Remote sensing of submerged vegetation canopies for biomass estimation. Int. J. Remote Sens. **14:** 10–16.

AUSTIN, A., AND R. ADAMS. 1978. Aerial and color infrared survey of marine plant resources. Photogramm. Eng. Remote Sens. **44:** 469–480.

BENTON, A. R., AND R. M. NEWMAN. 1976. Color aerial photography for aquatic plant monitoring. J. Aquat. Plant Manag. **14:** 14–16.

CHIVERS, R. C., N. EMERSON, AND D. R. BURNS. 1990. New acoustic processing for underway surveying. Hydrogr. J. **56:** 10–17.

CLARK, J. R. 1996. Coastal zone management handbook. CRC.

DENNISON, W. C., AND OTHERS. 1993. Assessing water quality with submersed aquatic vegetation: Habitat requirements as barometers of Chesapeake Bay health. Bioscience **43:** 86–94.

FELLEY, J. D., M. VECCHIONE, G. R. GASTON, AND S. M. FELLEY. 1989. Habitat selection by demersal nekton: Analysis of videotape data. Northeast Gulf Sci. **10:** 69–84.

FERGUSON, R. L., L. L. WOOD, AND D. B. GRAHAM. 1993. Monitoring spatial change in seagrass habitat with aerial photography. Photogramm. Eng. Remote Sens. **59:** 1033–1038.

GORDON, H. R., AND O. B. BROWN. 1974. Influence of bottom depth and albedo on the diffuse reflectance of a flat homogeneous ocean. Appl. Opt. **13:** 2153–2159.

———, AND K. DING. 1992. Self-shading of in-water optical instruments. Limnol. Oceanogr. **37:** 491–500.

HECK, K. L., J. R. PENNOCK, J. F. VALENTINE, L. D. COEN, AND S. A. SKLENAR. 2000. Effects of nutrient enrichment and small predator density on seagrass ecosystems: An experimental assessment. Limnol. Oceanogr. **45:** 1041–1057.

JOHNSON, P. E., M. O. SMITH, AND J. B. ADAMS. 1991. Simple algorithms for remote determination of mineral abundances and particle sizes from reflectance spectra. J. Geophys. Res. **97:** 2649–2658.

KIRKMAN, H., L. OLIVE, AND B. DIGBY. 1988. Mapping of underwater seagrass meadows. *In* Proceedings of the Symposium on Remote Sensing in the Coastal Zone, Department of Geographic Information, VA.2.1.–VA.2.9.

LANGTON, R. W., AND J. R. UZMANN. 1989. A photographic survey of the megafauna of the central and eastern Gulf of Maine. Fish. Bull. **87:** 945–954.

LEATHERS, R. A., T. V. DOWNES, AND C. D. MOBLEY. 2001. Self-shading correction for upwelling sea-surface radiance measurements made with buoyed instruments. Opt. Express **8:** 561–570.

———, AND N. J. MCCORMICK. 1998. Algorithms for ocean-bottom albedo determination from in-water natural-light measurements. Appl. Opt. **38:** 3199–3205.

LEE, Z., K. L. CARDER, S. K. HAWES, R. G. STEWARD, T. G. PEACOCK, AND C. O. DAVIS. 1994. Model for the interpretation of hyperspectral remote-sensing reflectance. Appl. Opt. **33:** 5721–5732.

———, ———, C. D. MOBLEY, R. G. STEWARD, AND J. S. PATCH. 1998. Hyperspectral remote sensing for shallow waters: 1. A semianalytical model. Appl. Opt. **37:** 6329–6338.

———, ———, ———, ———, AND ———. 1999. Hyperspectral remote sensing for shallow waters: 2. Deriving bottom depths and water properties by optimization. Appl. Opt. **38:** 3831–3843.

LEWIS, D. W. 1984. Practical sedimentology. Hutchinson Ross.

LEWIS, R. S., AND J. R. STONE. 1991. Lake Quaternary stratigraphy and depositional history of the Long Island Sound basin: Connecticut and New York. J. Coast. Res. **11:** 1–23.

LUCKHURST, B. E., AND K. LUCKHURST. 1978. Analysis of the influence of substrate variables on coral reef fish communities. Mar. Biol. **49:** 317–323.

LUCZKOVICH, J. J., T. W. WAGNER, J. L. MICHALEK, AND R. W. STOFFLE. 1993. Discrimination of coral reefs, seagrass meadows, and sand bottom types from space: A Dominican Republic case study. Photogramm. Eng. Remote Sens. **59:** 385–389.

LYZENGA, D. R. 1978. Passive remote sensing techniques for mapping water depth and bottom features. Appl. Opt. **17:** 379–383.

MALATESTA, R. J., P. J. AUSTER, AND B. P. CARLIN. 1992. Analysis of transect data for microhabitat correlations and faunal patchiness. Mar. Ecol. Prog. Ser. **87:** 189–195.

MARITORENA, S., A. MOREL, AND B. GENTILLI. 1994. Diffuse reflectance of oceanic shallow waters: Influence of water depth and bottom albedo. Limnol. Oceanogr. **39:** 1689–1703.

MOBLEY, C. D., AND OTHERS. 1993. Comparison of numerical models for computing underwater light fields. Appl. Opt. **32:** 7484–7504.

MUMBY, P. J., E. P. GREEN, A. J. EDWARDS, AND C. D. CLARK. 1997. Measurement of seagrass standing crop using satellite and digital airborne remote sensing. Mar. Ecol. Prog. Ser. **159:** 51–60.

NECKLES, H. A., R. L. WETZEL, AND R. J. ORTH. 1993. Relative effects of nutrient enrichment and grazing on epiphytic-macrophyte (*Zostera marina*) dynamics. Oecologia **93:** 285–295.

ORTH, R. J., AND K. A. MOORE. 1983. Submerged vascular plants: Techniques for analyzing their distribution and abundance. Mar. Tech. Soc. J. **17:** 38–52.

PARSONS, T. R., Y. MAITA, AND C. M. LALLI. 1984. A manual of chemical and biological methods for seawater analysis. Pergamon.

PHILPOT, W. D. 1987. Radiative transfer in stratified waters: A single-scattering approximation for irradiance. Appl. Opt. **26:** 4123–4132.

SABOL, D. E., J. B. ADAMS, AND M. O. SMITH. 1990. Predicting the spectral detectability of surface materials using spectral mixture analysis. *In* Proceedings of IGARRSS 1990, 13th Canadian Symposium on Remote Sensing **2:** 967–970.

SAVASTANO, K. J., K. H. FALLER, AND R. L. IVERSON. 1984. Estimating vegetation coverage in St. Joseph Bay, Florida, with an airborne multispectral scanner. Photogramm. Eng. Remote Sens. **50:** 1159–1170.

SCHLAGINTWEIT, G. E. O. 1993. Real-time acoustic bottom classification for hydrography: A field evaluation of Roxann. Canada Hydrographic Service.

SCHNEIDER, D. C., J. M. GAGNON, AND K. D. GILKISON. 1987. Patchiness of epibenthic megafauna on the outer Grand Banks of Newfoundland. Mar. Ecol. Prog. Ser. **39:** 1–13.

SHEPPARD, C. R. C., K. MATHESON, J. C. BYTHELL, P. MURPHY, C. BLAIR MEYERS, AND B. BLAKE. 1995. Habitat mapping in the Caribbean for management and conservation: Use and assessment of aerial photography. Aquat. Conserv. Mar. Freshw. Ecosyst. **5:** 277–298.

SNEDAKER, S. C., AND C. D. GETTER. 1985. Coastal resources management guidelines. Research Planning Institute.

SPITZER, D., AND R. W. J. DIRKS. 1987. Bottom influence on the reflectance of the sea. Int. J. Remote Sens. **8:** 279–290.

WAHLE, R. A., AND PECKHAM, S. H. 1999. Density-related reproductive trade-offs in the green sea urchin, *Strongylocentrotus droebachiensis.* Mar. Biol. **134:** 127–138.

WILLIAMS, S. L., AND M. H. RUCKELSHAUS. 1993. Effects of nitrogen availability and herbivory on eelgrass (*Zostera marina*) and epiphytes. Ecology **74:** 904–918.

ZAINAL, A. J. M., D. H. DALBY, AND I. S. ROBINSON. 1993. Monitoring marine ecological changes on the east coast of Bahrain with Landsat™. Photogramm. Eng. Remote Sens. **59:** 415–421.

ZIBORDI, G., AND G. M. FERRARI. 1995. Instrument self-shading in underwater optical measurements: Experimental data. Appl. Opt. **34:** 2750–2754.

Received: 2 October 2001
Accepted: 27 June 2002
Amended: 3 July 2002